Particle motion within the viscous sublayer of a turbulent shear flow

Guillaume Quibeuf, François Charru, Laurent Lacaze

Particle motion within the viscous sublayer of a turbulent shear flow

Guillaume Quibeuf, François Charru, and Laurent Lacaze

Institut de Mécanique des Fluides de Toulouse (IMFT) - Université de Toulouse, CNRS-INPT-UPS, Toulouse FRANCE

(Dated: July 8, 2021)

Abstract

The motion of isolated heavy particles on the bottom wall of a turbulent shear flow is investigated experimentally (using high frequency particle tracking), and correlated to that of the fluid (from high resolution LDV measurements). Numerous particle diameter, particle density and flow velocity are considered, where the particle remain within the viscous sublayer (particle Reynolds number lower than 10). It is shown that fluid flow fluctuations within the viscous sublayer (varying Couette flow) induce particle velocity fluctuations of same magnitude – slightly smaller –. The mean particle velocity, standard deviation and Lagrangian correlation time, are found to scale with the viscous scales. Particles roll and slide without takeoff, unlike what happens in viscous laminar flow where the lift force may overcome the immersed particle weight. Arguments are given for this difference. Probability density functions for the streamwise and spanwise velocity are found to follow Gamma and Gaussian laws, respectively, which also scale with the viscous scales.

I. INTRODUCTION

The shearing action of a water flow above a granular bed leads, for moderate shear stress, to bedload transport where particles move close to the bed. This transport has been extensively studied at a macroscopic level with emphasis on the mean sediment discharge, because the latter is the most relevant quantity for most applications (river morphodynamics, hydraulic engineering...). In this context, there exists a great variety of semi-empirical sediment transport laws derived from laboratory experiments [1]. However, their applicability range is quite narrow and discrepancy between predictions and *in situ* measurements can be large, especially for shear-stress close to threshold [2, 3]. These laws put forward the dominant effect of the fluid shear stress, as measured by the Shields number which represents the ratio of the hydrodynamic force on a particle to its immersed weight. However, they generally do not account for the weaker effect of particle inertia (as measured by the particle Reynolds number), nor the effect of other phenomena more difficult to control and model such as the bed packing density or heterogeneities of the particles shape and size.

Deeper insights have been achieved from studies at the grain scale, using particle tracking for the investigation of local dynamics, in viscous flows [4, 5] and turbulent streams [6, 7]. For the latter, detailed and time-resolved measurements of the near-bed fluid flow have improved our understanding of the interactions between turbulent structures and grain motion [8, 9] and their feedback on the flow [10–12].

The need of work on the motion of solitary grains – over a bed of sticked particles – appeared early, in order to get a deeper understanding of the hydrodynamic forces experienced by the grain, interactions with the bed (rebounds, momentum transfer, friction coefficient), and resulting trajectories. Quite different situations occur, from that of large grains (with Reynolds number of a few hundreds) saltating over the bed [13], to that of small particles reptating in viscous flows [14]. Other works were devoted to the problem of the flow conditions necessary to dislodge a grain out of the bed, showing in particular that the relevant quantity is the flow impulse (product of the instantaneous hydrodynamic force by its duration) rather than the force itself [15], or, equivalently, some energy transfer [16]. In another direction, attention has been paid to the motion of particles over *smooth* walls, in relation with industrial problems such as the cleaning of surfaces, filtration, or field-flow fractionation. Available studies typically provide correlations for the particle velocity as a function

of the friction velocity [17–19].

This paper reports an experimental investigation of the motion of isolated particles (small surface density) carried by a turbulent flow over a *smooth* bottom wall, for small particles lying within the viscous sublayer. The objective is to clarify the link between the dynamics and statistics of the near-wall fluid flow and those of individual grains, thanks to precise and reliable velocity measurements of both phases, and find their relevant scales. The experimental setup is first presented (Sec. II). Then results are given for the mean velocity, standard deviation, probability density functions and correlation times, for both the flow and the particles (Sec. III). Results are summarized in Sec. IV.

II. EXPERIMENTAL SET-UP

The experimental set-up, as sketched in Fig. 1, consists of a 5.59 m long duct with rectangular cross section with inner height $H = 59$ mm and width $B = 120$ mm. It is basically the same as that described in Ref. [20] with improvements given in Ref. [21]. The first 4.08 meters of the duct are made in Perspex, the end section (1.59 m long) where all experiments take place is made in a good quality glass in order to make observation easier. The duct is entirely filled with tap water (closed-conduit flow i.e. no free surface) and is pressurized by a 2 m high water column to avoid air bubble entrance. A divergent-honeycomb-convergent system homogenizes the turbulence at the entrance of the duct. The flow developpes along the Perspex part and one experimentally verified that it has reached a uniform regime (downstream invariance) at the end section. The flow rate is varied via a progressive cavity pump and monitored with an electromagnetic flow meter.

The duct Reynolds number $Re = \rho U_{\rm deb} D/\eta$ may reach 3×10^4, where $U_{\rm deb}$ is the mean fluid flow velocity, $D = 2BH/(B+H)$ the hydraulic diameter, $\rho = 10^3$ kg m^{-3} the water density and $\eta = \rho\nu = 10^{-3}$ Pa s its viscosity. The flow field was measured by Laser Doppler Velocimetry (Dantec Dynamics high power flowlite 2D system), in the vertical symmetry plane, at 4.2 m downstream of the entrance of the duct. The LDV probe, mounted on a 3-axis traverse system, permits to scan the flow along the vertical. Measurements were taken at every 0.05 mm within the first millimeter above the bottom wall, and at every millimeter above. The typical acquisition rate was about 100 Hz, with 5000 samples collected at each point.

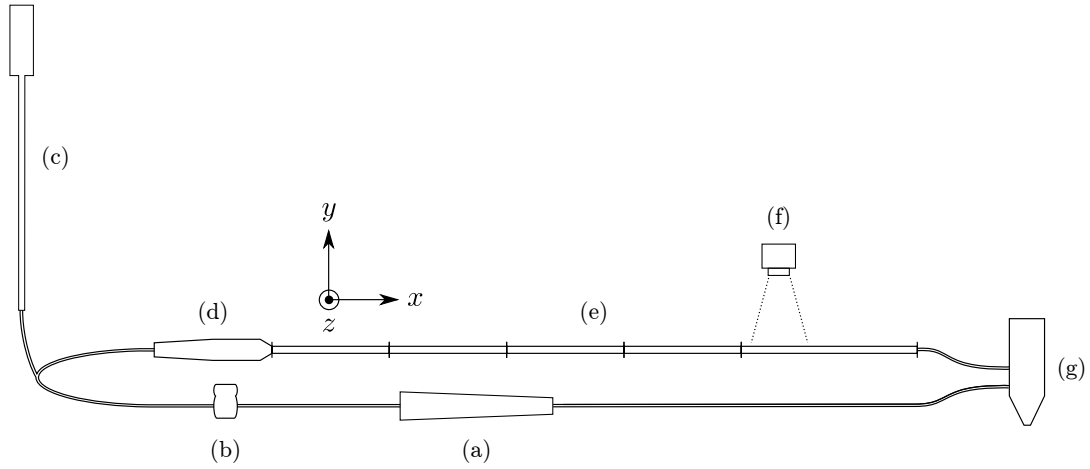

FIG. 1. Sketch of the experimental set-up. (a) Progressive cavity pump; (b) electromagnetic flow meter; (c) 2 m-high water column; (d) divergent, honeycomb and convergent; (e) duct with rectangular cross section; (f) movie camera; (g) sedimentation tank.

Let us decompose the streamwise fluid velocity as $u = \overline{u} + u'$ where $\overline{u}(y)$ is the time-averaged velocity and u' the fluctuation, with similar notations for the other velocity components. The wall shear stress τ_w, as determined from the near-wall slope of the mean velocity, $\tau_w = \rho\nu(\partial\overline{u}/\partial y)_{y\to 0}$, was found to agree with the Blasius correlation, $\tau_w/(\frac{1}{2}\rho U_{\rm deb}^2) = 0.0791\, Re^{-1/4}$ [20]. This correlation was used to compute the wall scales: the shear velocity $u_\tau = (\tau_w/\rho)^{1/2}$ and the viscous length $\delta_v = \nu/u_\tau$. Vertical profile of the mean velocity $\overline{u}^+(y^+)$, in wall units, are displayed in Fig. 2(a) for three Reynolds number. As expected,

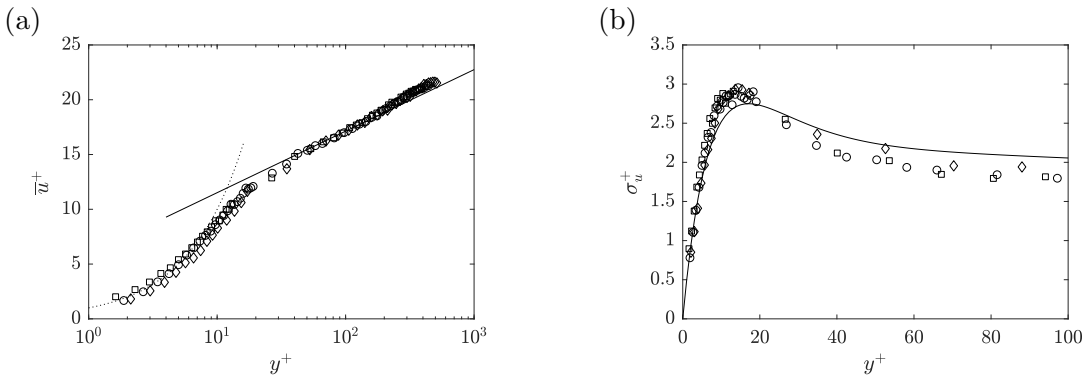

FIG. 2. Streamwise fluid velocity in the vertical symmetry plane, in wall units, for $Re = 18300$ (□), 21600 (○), 25000 (◇). (a) Mean velocity; (·····), $\overline{u}^+ = y^+$; (——), $\overline{u}^+ = 1/\kappa \log(y^+) + B$ with $\kappa = 0.41$ and $B = 5.9$. (b) Standard deviation $\sigma_u = \overline{u'^2}^{1/2}$; (——), Eq. (13) from Ref. 22.

Label	d (mm)	ρ_p (kg m^{-3})	Re	u_τ (mm s^{-1})	Re_p	θ
G1	0.13	2500	18300 - 25000	13.5 - 17.7	1.8 - 2.3	0.095 - 0.16
G2	0.31	2500	18300 - 25000	13.5 - 17.7	4.2 - 5.4	0.040 - 0.069
G3	0.54	2500	18300 - 25000	13.5 - 17.7	7.3 - 9.6	0.023 - 0.040
Z1	0.31	3800	20000 - 28300	14.6 - 19.8	4.5 - 6.1	0.025 - 0.046
Z2	0.54	3800	20000 - 26600	14.6 - 18.7	7.9 - 10.1	0.014 - 0.024

TABLE I. Beads diameter and density, and range of the hydrodynamical conditions explored.

velocity increases linearly from the wall within the viscous sublayer ($y^+ \lesssim 10$), and then logarithmically in the inertial range $40 \lesssim y^+ \lesssim 200$. The standard deviation $\sigma_u = \overline{u'^2}^{1/2}$, displayed in Fig. 2(b), reaches a maximum $\sigma_u^+ \approx 3$ at $y^+ \approx 15$ and then slowly decreases, in agreement with the semi-empirical relationship given by Ref. 22 (solid line).

The particles were white spherical glass or zirconium beads from Sigmund Lindner. Their density and median diameter d, after sieving, are given in Table I together with the explored ranges of the flow Reynolds number Re, friction velocity u_τ, particle Reynolds number $Re_p = u_\tau d/\nu$ and Shields number $\theta = \tau_w/((\rho_p - \rho)gd)$ (dimensionless wall shear stress). It can be seen that Re_p, which represents the particle diameter in wall units, is always below 10, which means that the particles remain within the viscous sublayer (of conventional thickness $11.6\,\delta_\nu$ [23]).

For a typical experiment, a few particles were released on the bottom wall of the duct (painted in black to enhance the contrast with the white particles), with surface density of a few particles per square centimeter. Their motion, as the flow was set out, was then followed by a CCD camera (Basler ace acA2040-180km, 2000×2000 pixels) placed above the last third of the duct length. The horizontal field of view was 18×18 mm^2 and the frame rate f was between 60 and 160 Hz. The images were then processed with a particle tracking algorithm[1] providing the particle trajectories and velocities. Note that the particles were observed in the central third of the duct width, where the influence of the lateral walls is quite negligible.

[1] from D. Blair and E. Dufresne, freely available at http://site.physics.georgetown.edu/matlab/.

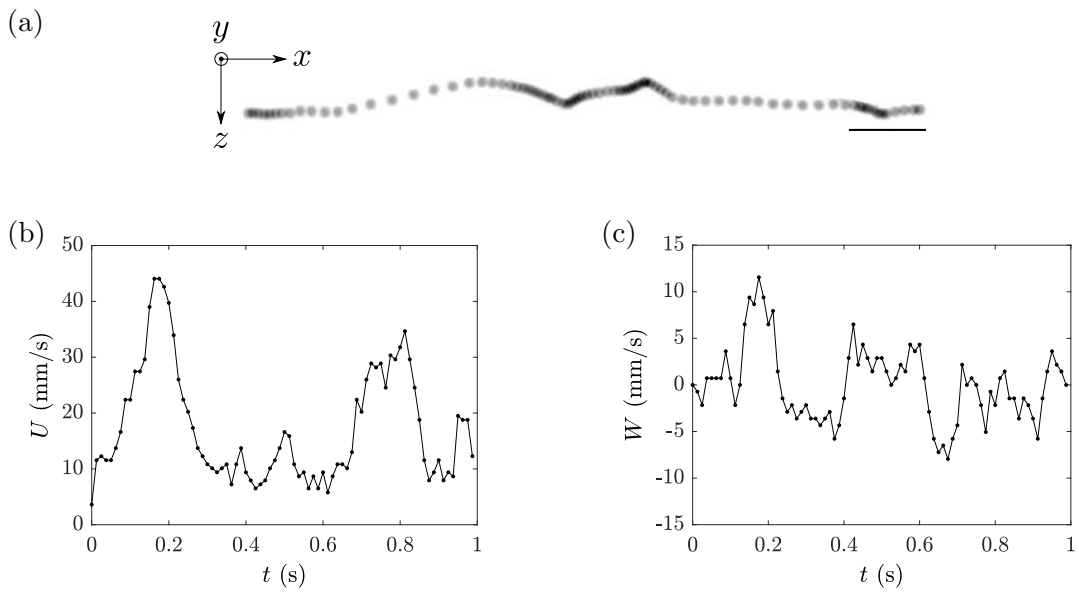

FIG. 3. (a) Chronophotography (from above, negative image) of a typical particle trajectory in the horizontal plane (the scale in the right bottom corner is 2 mm long); (b) and (c), corresponding streamwise and spanwise velocity components. Beads Z1 (see Table I), $u_\tau = 14.6$ mm s^{-1}, $Re_p = 4.8$, $f = 80$ Hz.

III. RESULTS

A. Particle trajectory and mean velocity

A typical particle trajectory in the horizontal plane, and the corresponding streamwise and spanwise velocity components, U and W, are shown in Fig. 3 for $Re_p = d^+ = 4.8$. It can be seen that the bead has an erratic motion with periods of sudden accelerations and decelerations, up to $3u_\tau$. This behavior, which was observed for all flow conditions, shows that although the particle lies within the viscous sublayer ($d^+ < 11.6$), its motion still reflects some unsteadiness of the turbulent flow.

Figure 4 displays the mean particle velocity $\overline{U}^+$, in wall units, for the five bead types (open symbols), as a function of the particle Reynolds number Re_p. It appears that all the data points fall onto the same curve, and that the particle velocity scales linearly with the Reynolds number, as

$$\overline{U}^+ = 0.26\, Re_p. \tag{1}$$

In other words, the mean particle velocity is $0.26\,\gamma d$, where $\gamma = u_\tau^2/\nu$ is the viscous shear

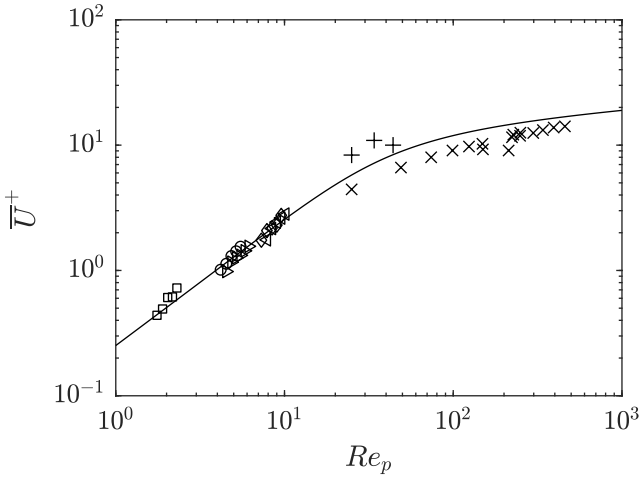

FIG. 4. Mean velocity $\overline{U}^+$ versus particle Reynolds number Re_p. Data for $Re_p \lesssim 10$ correspond to the present experiments: (□), beads G1; (○), beads G2; (◇), beads G3; (▷), beads Z1; (◁), beads Z2. Data for $Re_p \gtrsim 20$, (×) and (+), are from Refs. 18 and 19. (——), fit from from Ref. 18 (their Eq. 7).

rate close to the wall, i.e. it is equal to the fluid velocity at the distance $0.26\,d$ above the wall. Figure 4 also displays velocity measurements from Refs. 18 and 19, for $Re_p \gtrsim 20$ – where particles emerge out of the viscous sublayer in the buffer layer –, and a curve fitting their data. This curve corresponds to a semi-empirical law for the mean fluid velocity within the buffer layer, at the height $y = d$ above the wall, given by Eq. (7) in Ref. 18. When extrapolated down to the viscous sublayer, this law provides $\overline{u}^+ \sim 0.25\,d^+$, which no longer is the fluid velocity at the height $y = d$ (where it is $\overline{u}^+ = d^+$) but fits, by chance, the present particle velocities.

B. Assessment of a viscous flow model

Let us now compare the above particle velocity (1) with that found for isolated heavy particules in laminar viscous flow, by Leighton and coworkers [24, 25]. For their particles with small inertia, these authors identified three regimes. First, for low shear rates, the particle rolls on the wall with constant speed, without slipping. Then, slip occurs and the particle velocity increases. Eventually, for high shear rates, the lift force overcomes the immersed bead weight, the bead takes off and stabilizes at a finite (small) distance above the

wall. The dimensionless parameter that naturally emerges from the model, and governs both transitions, is Re_p^4/Re_s where $Re_s = V_s d/\nu$ is the settling Reynolds number (based on the Stokes settling velocity $V_s = (\rho_p - \rho)gd^2/18\eta$). The transitions to slipping and takeoff occur, with our notations, for $Re_p^4/Re_s \approx 1.6$ and $Re_p^4/Re_s \approx 32$, respectively (corresponding, with the notations of Refs. 24 and 25, to $Re_\gamma^2/Re_s \approx 0.2$ and $Re_\gamma^2/Re_s \approx 4$). The velocities and transitions measured in Refs. 24 and 25 were found to agree with an analytical calculation of the forces and torques on the particle, involving two parameters: a typical roughness size ϵd of the bead surface, $\epsilon \ll 1$, and a friction coefficient μ_f.

Figure 5 compares the present mean velocity measurements (data points) with the model of Refs. 24 and 25 (solid line), as a function of Re_p^4/Re_s. It can be seen that the agreement is good up to $Re_p^4/Re_s \approx 32$. For higher shear, the model predicts takeoff and higher particle velocity, whereas our observations do not reveal anything special: the velocity still scales with the shear rate u_τ^2/ν (constant $\overline{U}^+/Re_p$). The reason for the absence of any takeoff transition may be explained as follows. The lift force, as calculated in Refs 24 and 25, is the sum of six terms, each arising as the result of a pairwise combination of the translational velocity, rotational velocity, and the shear rate. These terms involve a numerical coefficient which may be positive (for four of them) or negative (for the last two). In turbulent flow, where particles experience a wide range of sliding and rolling motions, and shear rates, it can be expected that the resulting mean lift-force be very small, with either positive or negative sign. Hence the absence of takeoff transition observed in Fig. 5 for our experiences, unlike what happens in laminar flow. This explanation also corroborates direct visual observation, which seem to indicate that particles always keep contact with the wall.

C. Standard deviations of the particle velocity and fluid velocity

It is well-known that heavy particles moving on a wall in turbulent flow may experience large velocity fluctuations, see e.g. Ref. 17. We explore here more thoroughly the statistics of these fluctuations and assess their correlation with those of the fluid. Figure 6(a) displays the standard deviation of the streamwise velocity σ_U (or r.m.s velocity, filled symbols). (The mean velocities $\overline{U}^+$ previously shown in Fig. 4 are shown again, with open symbols, for easier comparison.) It can be seen that all standard deviations fall close to the curve

$$\sigma_U^+ = 0.15\, Re_p \tag{2}$$

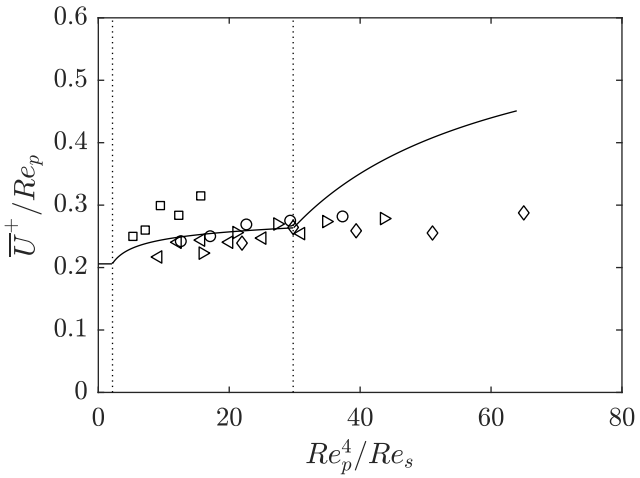

FIG. 5. Mean particle velocity $\overline{U}^+$ as a function of the shear parameter Re_p^4/Re_s, and theoretical calculation (solid line) by Ref. 24 and 25 for relative roughness $\epsilon = 0.005$ and friction coefficient $\mu_f = 0.25$. The vertical dashed lines locate the rolling-slipping and takeoff transitions predicted by the model. (□), beads G1; (○), beads G2; (◇), beads G3; (▷), beads Z1; (◁), beads Z2.

(dotted line in the figure). Thus, σ_U^+ scales with the particle Reynolds number, as the mean velocity $\overline{U}^+$, and represents a large part of the latter, of about 60%. These results show that, although the Reynolds stresses are small within the viscous sublayer, large fluctuations may however exist there.

Figure 6(b) compares σ_U to the r.m.s. fluid velocity, σ_u, at the height of the center of the particle, $y = \frac{1}{2}d$. It can be seen that σ_U increases approximately linearly with σ_u, and is always smaller, according to

$$\sigma_U \approx 0.7\,\sigma_u(y = 0.5d). \tag{3}$$

Closer inspection shows that the r.m.s. velocity is slightly smaller for the heavy zirconium beads than for the lighter glass ones, which may be interpreted as a filtering effect due to particle inertia. The present fluid measurements agree with previous direct measurements of the wall shear-stress [26] which showed that fluctuations may represent 40% of the mean shear. These fluctuations likely correspond to the streamwise elongated streaks of alternating fast and slow fluid that meander in the near-wall region, below $y^+ \approx 100$ [27].

Now consider the fluctuations of the spanwise velocity, σ_W. Distributions (not shown) were found to be Gaussian, consistently with previous findings for a particle on a rough bed in viscous flow [14]. Fig. 7 shows that, in wall units, σ_W^+ scales with the particle Reynolds

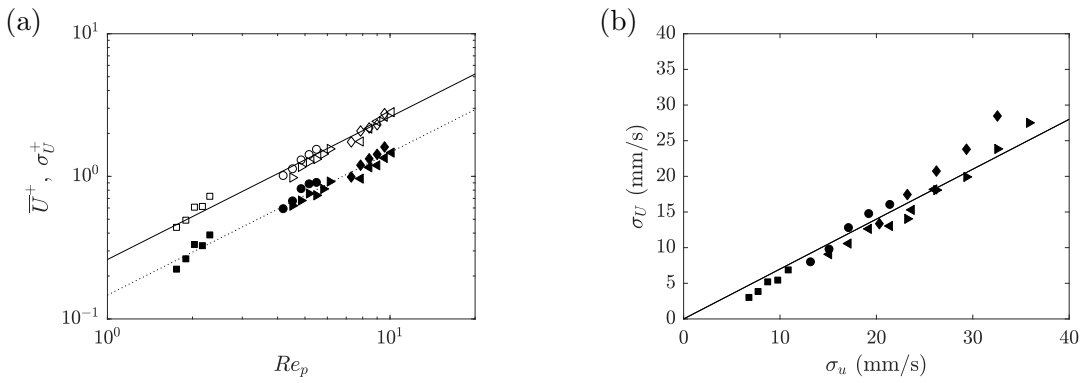

FIG. 6. (a) r.m.s. fluctuations σ_U^+ (filled symbols) and mean streamwise velocity $\overline{U}^+$ (open symbols), in wall units, as a function of the particle Reynolds number Re_p. Symbols: see Fig. 5; (——), Eq. (1). (·····), Eq. (2). (b) σ_U versus the r.m.s. fluid velocity σ_u at the height $y = \frac{1}{2}d$.

number Re_p (i.e, σ_W scales with the viscous velocity $u_\tau^2 d/\nu$, as the streamwise component). However, a particle density effect here appears: for the same Re_p, the r.m.s. velocity is much smaller for the heavy zirconium beads. In other words, heavy particles, with larger inertia, resist more strongly to spanwise fluid velocity fluctuations. A general correlation accounting for this inertia effect, also reported in Fig. 7, is

$$\sigma_W^+ = 0.21 \, \frac{\rho}{\rho_p} \, Re_p. \tag{4}$$

D. Probability density functions

Now turn to the probability density functions (PDF) of the fluid and particle streamwise velocities. Figure 8(a) displays, for five values of the Reynolds number, the normalized PDF of the dimensionless fluid velocity u^+ at the height $y = 0.31$ mm (which corresponds to the diameter of the beads G2). It can be seen that all the data points fall onto a single curve, which shows that all statistics within the viscous sublayer scale with the wall units.

PDF of the grain velocities were computed, for each flow velocity, from typically 650 trajectories corresponding to a number of about 50×10^3 samples. Figure 8(b) displays, for the beads G2 and five values of the Reynolds number, the normalized PDF of the normalized velocity $U/\gamma d = U^+/Re_p$ (with γ the shear rate in the viscous sublayer). It can be seen that, for $U^+/Re_p \lesssim 0.5$, all the data points fall onto a single curve, confirming that

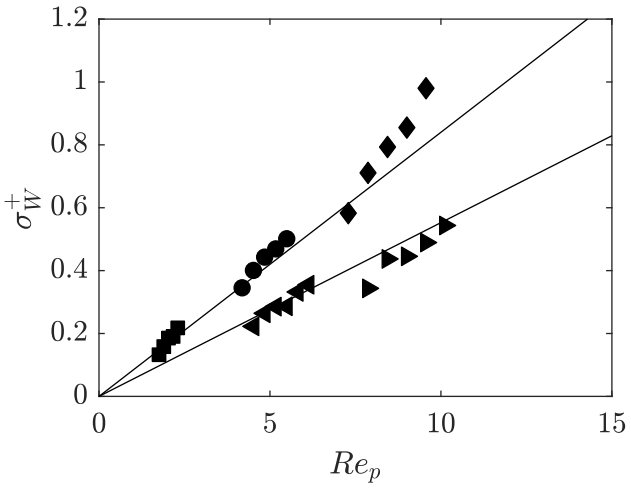

FIG. 7. Standard deviation of the spanwise velocity, σ_W^+, as a function of the particle Reynolds number Re_p; the lines correspond to Eq. (4). (□), beads G1; (○), beads G2; (◇), beads G3; (▷), beads Z1; (◁), beads Z2.

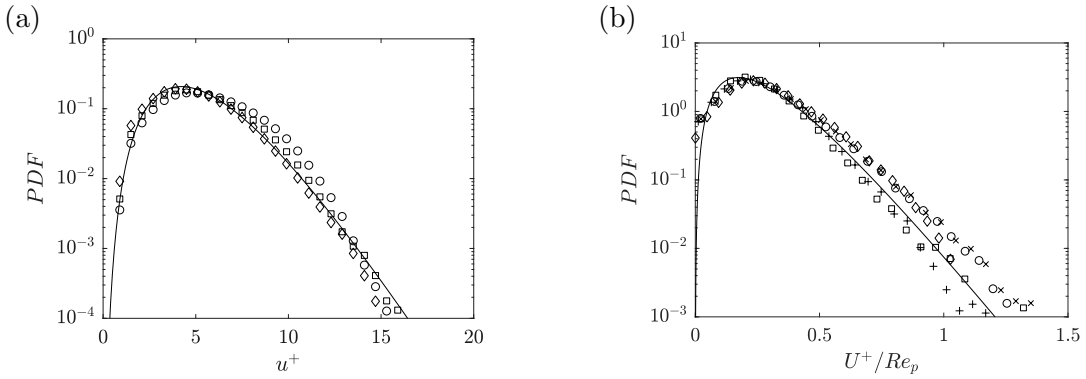

FIG. 8. Probability density functions of the streamwise velocity: (a), fluid at the height $y = 0.31$ mm; (b), particles G2 with diameter $d = 0.31$ mm. (□) $Re = 18300$, (+) $Re = 20000$, (○) $Re = 21600$, (×) $Re = 23300$, (◇) $Re = 25000$. (——), Gamma distributions, see Eq. (5).

the particle motion scales with the viscous units with negligible inertia effect. However, for $U^+/Re_p \gtrsim 0.5$, which corresponds to velocity larger than twice the mean ($\overline{U}^+/Re_p = 0.26$), the PDF separate, without, however, any clear trend with the Reynolds number variations.

The solid lines in Figs. 8(a) and 8(b) correspond to the Gamma distributions with PDF:

$$PDF(X) = \frac{1}{b^a \Gamma(a)} X^{a-1} \mathrm{e}^{-X/b}, \tag{5}$$

where X stands either for u^+ or U^+/Re_p, Γ is the Gamma function, and $a = \overline{X}^2/\sigma_X^2$ and

$b = \sigma_X^2/\overline{X}$ are the two parameters of the distribution [23]. For the fluid (Fig. 8(a)), fitting measurements with Eq. (5) provides $a = 5.95$ and $b = 0.85$. For the particles (Fig. 8(b)), the parameters are $a = 3.0$ and $b = 0.086$, as deduced from Eqs. (1) and (2). It is noticeable that both PDF, for the fluid and the grains, are well described by Gamma distributions. The positive skewness of these distributions, very common in near-wall turbulence, is considered as the signature of sweeps [28–31]. Regarding the grains, Gamma laws have been previously evidenced in Ref. 19 (for shear higher than here) with long tails associated with the large velocities attained during small saltation jumps. Here, particles rather roll and slide in close contact with the wall (see the previous dicussion of Fig. 5). Such Gamma distributions of the particle velocity, with close resemblance with those for the fluid, show that particles follow the fluid fluctuations, consistently with the previous result that the mean and r.m.s. velocities scale with the viscous velocity $\gamma d = u_\tau^2 d/\nu$.

E. Correlation times

A last viscous argument may now be added to the above results, involving correlation times. Let us consider the autocorrelation function

$$R_{XX}(\tau) = \frac{1}{\sigma_X^2}\overline{X(t)X(t+\tau)} \tag{6}$$

where X stands either for the velocity fluctuations u' or U', τ is the time lag and the overbar still denotes temporal average. Figure 9(a) displays, for five Reynolds numbers, the autocorrelation function of the fluid velocity at the height $y = 0.31$ mm (equal to the diameter of the beads G2). Similarly, Fig. 9(b) displays the autocorrelation function of the particle velocity, averaged over numerous trajectories. All plots in both figures display similar decrease with the time lag τ, with similar timescales a few hundreds of milliseconds. The higher the duct Reynolds number is, the shorter the timescale for both the fluid and the particles.

More quantitatively, a correlation time τ_c can be defined as the time lag where the autocorrelation has decreased to some conventional value, here of 0.2, corresponding, in Fig. 9, to the dotted lines (we have checked that choosing other values of the cut-off do not alter the conclusions to be drawn). Figure 10 displays the correlation times for the fluid (filled symbol) and all grain types (open symbols). They appear to decrease with the

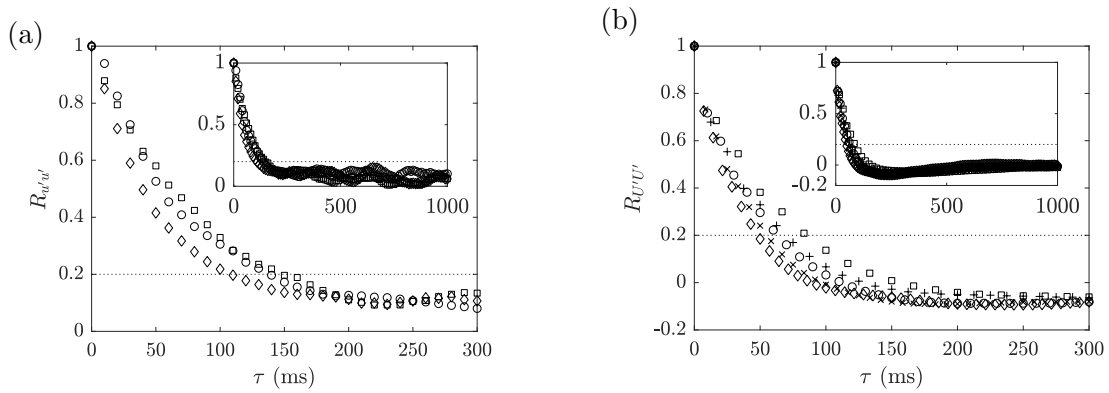

FIG. 9. Autocorrelation functions of the streamwise r.m.s. velocity. (a), fluid at the height $y = 0.31$ mm; (b), glass beads with $d = 0.31$ mm. Insets: long time behavior. (□) $Re = 18300$, (+) $Re = 20000$, (○) $Re = 21600$, (×) $Re = 23300$, (◇) $Re = 25000$.

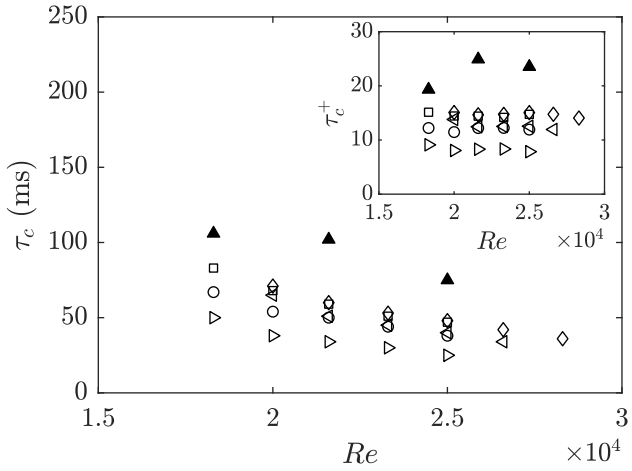

FIG. 10. Correlation times of the streamwise velocity of the fluid (▲) and grains (open symbols, see the caption of Fig. 5) with the duct Reynolds number. Inset : correlation times in wall units.

Reynolds number, those of the beads being about one-half that of the fluid. No clear trend can be seen from one grain type to the other, as the grain density or diameter varies. The inset in Fig. 10 displays the same times once normalized with the viscous time $\gamma^{-1} = \nu/u_\tau^2$. The dimensionless times now appear quasi constant with the duct Reynolds number, as expected, with $\gamma\tau_c$ in the range 20-25 for the fluid and 10-15 for the grains. As a hint, the distance travelled by a grain with mean velocity $0.26\,\gamma d$ during the correlation time $15\,\gamma^{-1}$ provides a correlation distance of about four diameters.

IV. SUMMARY AND CONCLUSION

The experimental study reported in this paper shows that in a turbulent boundary layer, the motion of heavy particles with Reynolds number $Re_p = u_\tau d/\nu$ lower than 10 (i.e. particles within the viscous sublayer of characteristic thickness $11.6\,\nu/u_\tau$) closely follow fluid fluctuations (unsteady and space-varying Couette flow with mean shear rate $\gamma = u_\tau^2/\nu$). Consequently, all velocity statistics – mean velocity, standard deviation, PDF – scale with the viscous velocity $\gamma d = u_\tau^2 d/\nu = u_\tau\, Re_p$ which corresponds to the mean fluid velocity at the distance d above the wall. In particular, the mean streamwise particle velocity was found to be $\overline{U} \approx 0.26\,\gamma d$ and its standard deviation $\sigma_U \approx 0.15\,\gamma d$. Accordingly, the correlation time was found to be $15\,\gamma^{-1}$, corresponding to a correlation distance of about four particle diameters.

Although the above scalings indicate small particle inertia, the spanwise motion was found to be affected by the particle density, with standard deviation proportional to the density ratio ρ/ρ_p (i.e. smaller for heavier particles, as expected).

The fact that the particle velocity scales with the fluid velocity γd indicates that, within the explored range of flow conditions, particles do not take off and keep contact with the bed. This result, which is consistent with visual observations, was assessed by comparison with a theoretical model for a particle in (steady) laminar flow. Indeed, this model, validated with previous experiments, predicts that beyond some particle Reynolds number, the lift force on the particle exceeds its immersed weight. Then, the particle takes off, and its velocity departs from the previous viscous scaling, which phenomenon was not observed here. Then it can be argued from the structure of the expression of the lift force (see the discussion in the previous section) that in the unsteady and space-varying Couette flow taking place in the viscous sublayer, the positive and negative contributions to the lift force nearly cancel, so that takeoff cannot occur.

As a conclusion, it can be said that further investigations are now needed in order to understand how the above conclusions may be altered for larger particles emerging out of the viscous sublayer, on the one hand, and for particles over a rough wall, on the other hand.

---

[1] H. Chanson, *Hydraulics of open channel flow: an introduction* (Arnold, 1999).

[2] T. Nakato, "Tests of selected sediment-transport formulas," J. Hydr. Engrg **116**, 362 (1990).

[3] J. C. Bathurst, "Effect of coarse surface layer on bed-load transport," J. Hydr. Engrg **133**, 1192 (2007).

[4] F. Charru, E. Larrieu, J. B. Dupont, and R. Zenit, "Motion of a particle near a rough wall in a viscous shear flow," J. Fluid Mech. **570**, 431 (2007).

[5] H. Mouilleron, F. Charru, and O. Eiff, "Inside the moving layer of a sheared granular bed," J. Fluid Mech. **628**, 229–239 (2009).

[6] E. Lajeunesse, L. Malverti, and F. Charru, "Bed load transport in turbulent flow at grain scale : experiments and modeling," J. Geophys. Res. **115**, F04001 (2010).

[7] J. Shim and J. G. Duan, "Experimental study of bed-load transport using motion tracking," Int. J. Sediment Res. **32**, 73 (2017).

[8] J. M. Nelson, R. L. Shreve, S.R. McLean, and T. G. Drake, "Role of the near-bed turbulence structure in bed load transport and bed form mechanics," Water Resources Res. **31**, 2071 (1995).

[9] J. Lelouvetel, F. Bigillon, D. Doppler, I. Vinkovic, and J.-Y. Champagne, "Experimental investigation of ejections and sweeps involved in particle suspension," Water Resources Res. **45**, W02416 (2009).

[10] A. Gyr and A. Schmid, "Turbulent flows over smooth erodible sand beds in flume," J. Hydr. Res. **35**, 525 (1997).

[11] L. Campbell, I. McEwan, V. Nikora, D. Pokrajac, M. Gallagher, and C. Manes, "Bed-load effects on hydrodynamics of rough-bed open-channel flows," J. Hydr. Engrg **131**, 576 (2005).

[12] S. Dey, S. Sarkar, and L. Solari, "Near-bed turbulence characteristics at the entrainment threshold of sediment beds," J. Hydr. Engrg **137**, 945 (2011).

[13] J. R. D. Francis, "Experiments on the motion of solitary grains along the bed of a water stream," Proc. R. Soc. Lond. A **332**, 443–471 (1973).

[14] F. Charru, H. Mouilleron, and O. Eiff, "Erosion and deposition of particles on a bed sheared by a viscous flow," J. Fluid Mech. **519**, 55–80 (2004).

[15] A. O. Celik, P. Diplas, C. L. Dancey, and M. Valyrakis, "Impulse and particle dislodgement under turbulent flow conditions," Phys. Fluids **22**, 046601 (2010).

[16] M. Valyrakis, P. Diplas, and C. L. Dancey, "Entrainment of coarse particles in turbulent flows: An energy approach," J. Geophys. Res: Earth Surfaces **118**, 42–53 (2013).

[17] P. Sechet and B. Le Guennec, "Bursting phenomenon and incipient motion of solid particles in bed-load transport," J. Hydr. Res. **37**, 683 (1999).

[18] P. Y. Julien and B. Bounvilay, "Velocity of rolling bed load particles," J. Hydr. Engrg **139**, 177 (2013).

[19] J. Campagnol, F. Ballio, S. A. Hosseini Sadabadi, and H. Sazadul, "Particle motion of bed-load sediment moving over a smooth bed," in *Proc. Int. Conf. Fluvial Hydraulics, RIVER FLOW 2014* (2014) p. 763.

[20] E. M. Franklin and F. Charru, "Subaqueous barchan dunes in turbulent shear flow. Part 1. Dune motion," J. Fluid Mech. **675**, 199 (2011).

[21] G. Quibeuf, *Étude expérimentale du transport sédimentaire hors équilibre*, Ph.D. thesis, Université de Toulouse (2019).

[22] I. Nezu and W. Rodi, "Open-channel flow measurements with a laser doppler anemometer," J. Hydr. Engrg **112**, 335–355 (1986).

[23] S. B. Pope, *Turbulent Flows* (Cambridge Univ. Press, 2000).

[24] G. P. Krishnan and D. T. Leighton, "Inertial lift on a moving sphere in contact with a plane wall in a shear flow," Phys. Fluids **7**, 2538–2545 (1995).

[25] M. R. King and D. T. Leighton, "Measurement of the inertial lift on a moving sphere in contact with a plane wall in a shear flow," Phys. Fluids **9**, 1248–1255 (1997).

[26] L. Keirsbulck, L. Labraga, and M. Gad el Hak, "Statistical properties of wall shear stress fluctuations in turbulent channel flows," Int. J. Heat Fluid Flow **37**, 1 (2012).

[27] C. R. Smith and S. P. Metzler, "The characteristics of low-speed streaks in the near wall region of a turbulent boundary layer," J. Fluid Mech. **129**, 27 (1983).

[28] Z. Zarić, "Statistical analysis of wall turbulence phenomena," Advances Geophys. **18**, 249 (1975).

[29] F. Durst, J. Jovanovic, and Lj. Kanevce, "Probability density distribution in turbulent wall boundary-layer flows," in *Turbulent Shear Flows 5* (1987) p. 197.

[30] J. M. Österlund, *Experimental studies of zero pressure-gradient turbulent boundary layer flow*, Ph.D. thesis, KTH Royal Institute of Technology (1999).

[31] Boo C. Khoo, Y T. Chew, and C Teo, "Near-wall hot-wire measurements. part II : Turbulence time scale, convective velocity and spectra in the viscous sublayer," Exp. Fluids **31**, 494 (2001).